Materials Transactions, Vol. 51, No. 9 (2010) pp. 1663 to 1670

Applicability of Weibull Distribution to Description of Distributed Normalized Critical Current of Bent-Damaged Bi2223 Composite Tape

Shojiro Ochiai[1], Hiroshi Okuda[1], Michinaka Sugano[2], Masaki Hojo[3], Kozo Osamura[4], Tsuneo Kuroda[5], Hiroaki Kumakura[5], Hitoshi Kitaguchi[5], Kikuo Itoh[5] and Hitoshi Wada[5]

[1]*Department of Materials Science and Engineering, Kyoto University, Kyoto 606-8501, Japan*
[2]*Department of Electronic Science and Engineering, Kyoto University, Kyoto 615-8530, Japan*
[3]*Department of Mechanical Engineering and Science, Kyoto University, Kyoto 606-8501, Japan*
[4]*Research Institute for Applied Sciences, Kyoto 606-8202, Japan*
[5]*Superconducting Materials Center, National Institute for Materials Science, Tsukuba 305-0047, Japan*

Critical current of bent-damaged Bi2223 composite tape differs from specimen to specimen. To describe the distributed critical current values of specimens, the three-parameter Weibull distribution function has been employed and has been demonstrated to describe the experimental results. In the present work, the reason for this was discussed by modeling analysis of the experimental results in a round robin test of VAMAS/TWA16. The distribution of the measured normalized critical current values was described well by using the damage evolution approach, in which the difference in damage evolution among the specimens was correlated to the distribution of critical current values. From this approach, the three-parameter Weibull distribution function for critical current values was derived, which gave almost the same parameter values for the minimum critical current, scale parameter and shape parameter as those obtained by the direct application of the Weibull distribution function to the experimental results. Based on this result, the reason why the normalized critical current values of bent-damaged composite tape is described by the three-parameter Weibull distribution function was accounted for in a quantitative manner by the difference in damage evolution among the specimens. [doi:10.2320/matertrans.MAW201001]

(Received March 25, 2010; Accepted June 17, 2010; Published August 4, 2010)

Keywords: *Bi2223 composite superconductor, critical current distribution, bending, heterogeneous damage, Weibull distribution*

1. Introduction

The critical current of Bi2223/Ag/Ag alloy composite tape under externally applied strain is known to be reduced first at the irreversible strain at which the damage of the Bi2223 filaments takes place, and then to be further reduced with increasing strain due to damage evolution.[1–14] Heterogeneous damage occurs, and the damage evolution behavior differs from specimen to specimen and from location to location within a specimen.[9–14] Accordingly, when a number of specimens are tested, the critical current differs from specimen to specimen.

To describe the damage-induced distribution of critical current of the bent specimens, we have recently proposed a modeling approach that incorporates the correlation among the critical current, the shape of the core where the Bi2223 filaments are embedded, the applied bending strain and the damage evolution.[11,12,14] In this approach, the $\varepsilon_f - \varepsilon_r$ value, where ε_f is the fracture strain of the bare Bi2223 filaments and ε_r is the residual strain of the filaments in the current transport direction, was treated as a variable; using this value, the difference in damage amount among the specimens was expressed. The $\varepsilon_f - \varepsilon_r$ value corresponds to the tensile strain at which the filaments embedded in the composite tape are fractured. Because the ε_r is negative (compressive) in the Bi2223 composite tape, as has been demonstrated by X ray diffraction analysis,[7,8] the actual fracture strain of the filaments in the composite tape is by $-\varepsilon_r$ higher than the intrinsic fracture strain ε_f of the filaments alone.[2,4,6–8,11,14] The $\varepsilon_f - \varepsilon_r$ value is different from location to location within a specimen as well as from specimen to specimen. In the preceding works,[11,12] the heterogeneous damage behavior was formulated by the distributed $\varepsilon_f - \varepsilon_r$ values and was correlated to the distribution of critical current values. The procedure for application and the features of this approach (hereinafter "damage approach") is presented later in Section 3.2. This approach was applied to the measured values of the VAM1 sample in the round robin test[10] of VAMAS (Versailles project on advanced materials and standard)/TWA 16 (Technical working area 16, superconducting materials). It was shown that the measured distribution of the critical current values is described well by this approach. However, the calculation was carried out only numerically and the distinct distribution function could not be derived in the preceding works. In the present work, this approach was used extensively to obtain the distinct distribution function of the critical current of bent-damaged Bi2223 composite tape.

The outline of the present work is as follows. When the Weibull distribution is applied directly to the measured normalized critical current values (I_c/I_{c0} where I_c is the critical current at arbitrary bending strain ε_B and I_{c0} is the original critical current at $\varepsilon_B = 0$) for the VAM1 sample, the Weibull parameters characterizing the distribution can be obtained empirically by curve fitting. This approach is called as "Weibull approach", hereinafter. The result of application of Weibull approach is presented in Section 4.1. Then the damage approach is applied to the same data. It is shown in Section 4.2 that the damage approach gives the same result as the Weibull approach. The reason why the distribution of I_c/I_{c0} values of the bent-damaged specimens is described by the Weibull distribution function is discussed in 4.3, considering the formulation of the distribution function derived from the damage approach.

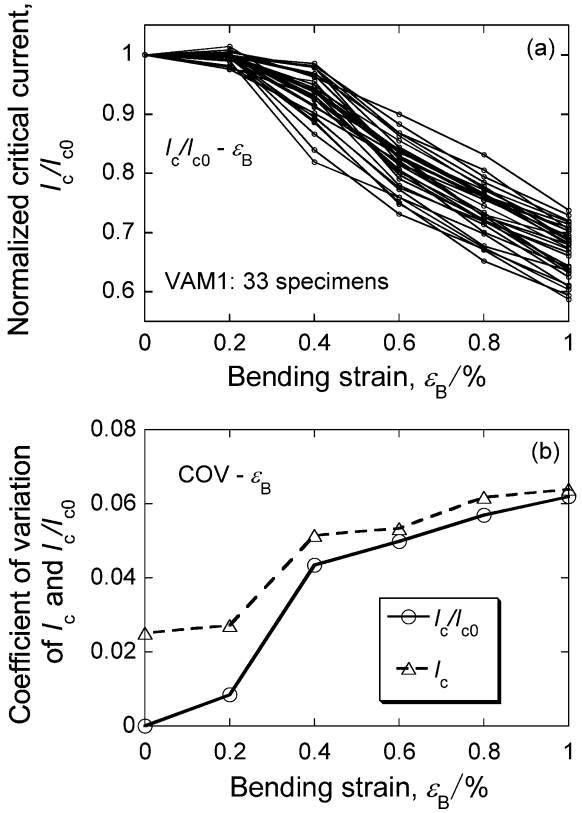

Fig. 1 Variation of (a) normalized critical current I_c/I_{c0} and (b) coefficient of variation (COV) of I_c/I_{c0} and I_c values with increasing bending strain ε_B, measured for 33 specimens.[10,11]

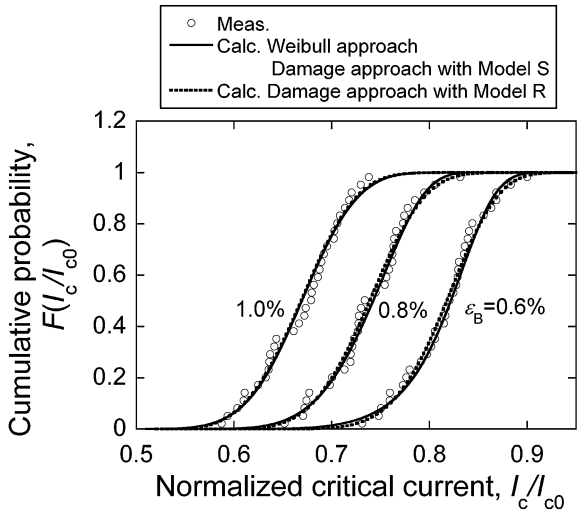

Fig. 2 Cumulative probability F of measured critical current I_c/I_{c0} at $\varepsilon_B = 0.6$, 0.8 and 1.0%. Solid curves show the results analyzed using the direct Weibull approach and the damage approach with Model S, which were on the same curves. Broken curves show the calculation results from eq. (9) based on the damage approach with Model R.

2. Data for Analysis

Figure 1 shows the variation of (a) the normalized critical current I_c/I_{c0} and (b) COV (coefficient of variation) of I_c/I_{c0} values with increasing bending strain ε_B for 33 specimens, measured for VAM1 sample in the round robin test[10] of VAMAS/TWA 16. The test specimens had width (W) of 3.70 mm and thickness (t) of 0.270 mm on average. In the measurement of the critical current of bent samples in the round robin test, bending strain was applied at room temperature by pressing the sample with the upper GFRP (glass fiber reinforced plastic) die to the lower one with the same curvature. The bending strain ε_B (= tensile strain of the outer surface of the composite on the tensile side) was given by $\varepsilon_B = t/(2R)$ where t is the overall thickness of the sample and R is the radius of the die. The specimens bent at room temperature were cooled down to 77 K, and the critical current I_c was measured with a criterion of 1 μV/cm in a self-magnetic field. The distance between the voltage taps was 30 mm. Details of the test procedure were reported in Ref. 10).

In the high bending strain range of $\varepsilon_B = 0.6$–1.0% where all specimens have been damaged, the COV of I_c values is close to that of I_c/I_{c0} (Fig. 1(b)). This suggests that the difference in the extent of damage among the specimens is responsible for the distribution commonly of I_c and I_c/I_{c0} at high bending strains. In the present work, we focused on the distribution of I_c/I_{c0} values of the bent-damaged specimens, and the I_c/I_{c0} values at $\varepsilon_B = 0.6$, 0.8 and 1.0% were taken up for analysis. The cumulative (F) and density (f) probability of the critical current (I_c/I_{c0}) values at $\varepsilon_B = 0.6$, 0.8 and 1.0%, taken from Fig. 1(a), are presented in Figs. 2 and 3, respectively. The results shown in Figs. 2 and 3 were analyzed by the Weibull approach and the damage approach.

3. Procedure for Analysis

3.1 Description of the distribution of I_c/I_{c0} values by means of the Weibull approach

The three parameter Weibull distribution function has been proposed originally to describe the strength distribution of materials.[15] This function has been used to describe the transport critical current distribution[11–14] and the critical current distribution at weak links for analysis of V (voltage)–I (current) curve near the transition from superconducting to normal conductive state.[16,17] The three-parameter Weibull distribution function is characterized by three parameters ($(I_c/I_{c0})_{min}$ is the minimum (lower limit) value of critical current, $(I_c/I_{c0})_0$ is the scale parameter, and m is the shape parameter). With these parameters, the cumulative probability F of the critical current (I_c/I_{c0}) is expressed by

$$F(I_c/I_{c0}) = 1 - \exp\left[1 - \left\{\frac{I_c/I_{c0} - (I_c/I_{c0})_{min}}{(I_c/I_{c0})_0}\right\}^m\right] \quad (1)$$

The values of $(I_c/I_{c0})_{min}$, m and $(I_c/I_{c0})_0$ in eq. (1) which describe the measured distributions at $\varepsilon_B = 0.6$, 0.8 and 1.0% were estimated by the regression analysis, as shown in Section 4.1.

3.2 Description of the distribution of I_c/I_{c0} values by means of the damage approach

Figure 4(a) shows a micrograph of the transverse cross-section of the sample. When the thickness direction is enlarged by a factor of 3, the shape of the core (the region in which Bi2223 filaments are embedded in Ag) can be more clearly observed, as shown in Fig. 4(b).

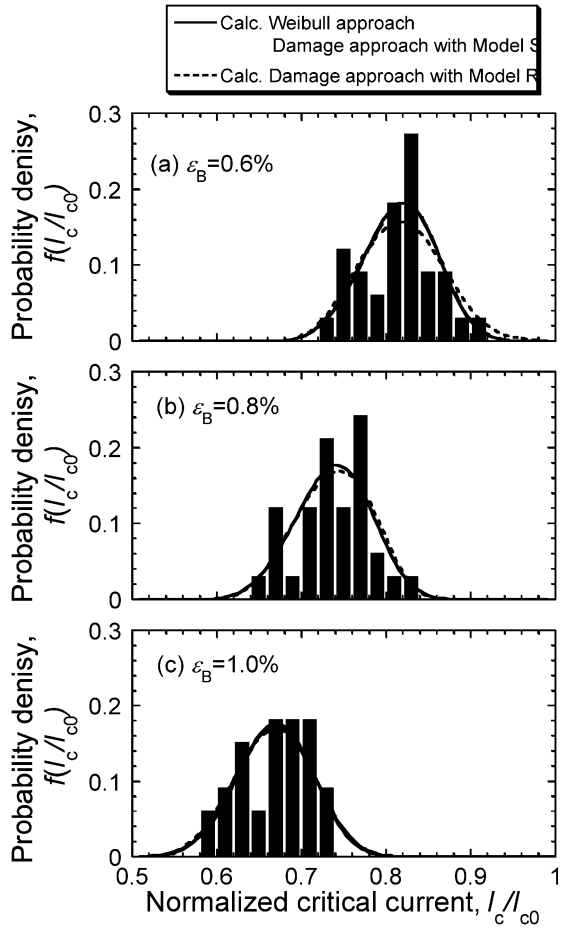

Fig. 3 Probability density f of measured critical current I_c/I_{c0} at $\varepsilon_B = 0.6$, 0.8 and 1.0%. Solid curves show results analyzed using the direct Weibull approach and the damage approach with Model S, which were on the same curves. Broken curves show the calculation results from eq. (9) based on the damage approach with Model R.

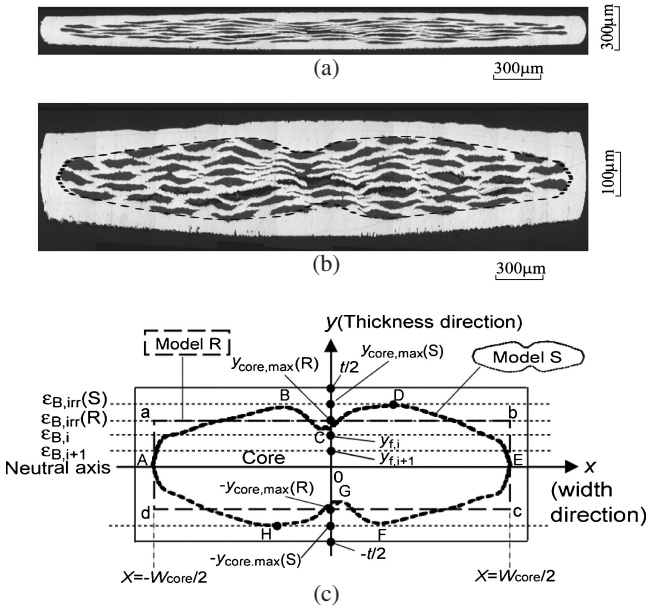

Fig. 4 Transverse cross-section of the composite tape. (a) Optical micrograph in the as-observed state and the shape of the core. (b) Deformed optical micrograph, where the thickness direction is expanded by a factor 3; broken curve shows the core boundary. (c) Schematic representation of the geometry of the cross-section in relation to the damage extension. Damage occurs first at the outermost filaments at the maximum value of y_{core} ($y_{core,max}$) when the bending strain ε_B reaches the irreversible bending strain $\varepsilon_{B,irr}$. When the bending strain ε_B is raised from $\varepsilon_{B,irr}$ to $\varepsilon_{B,i}$ and then to $\varepsilon_{B,i+1}$, the damage front y_f moves from $y_{core,max}$ to $y_{f,i}$ and then to $y_{f,i+1}$.

As the damage of the Bi2223 filaments existing in the core causes the reduction in critical current, it is necessary to formulate the shape. Taking the width- and thickness-directions of the composite tape as the x- and y-axes, respectively, and the center of the composite tape as $x = y = 0$ (Fig. 4(c)), and denoting the y-coordinate of the boundary of the core as y_{core}, we formulated y_{core} as a function of x in two models. One is the actual shape-incorporated model with the core boundary ABCDEFGHA in Fig. 4(c), which is referred to as Model S. This model is rigid but requires a relatively long time for calculation. Another model is used where the shape of the core is approximated as a rectangle (abcd in Fig. 4(c)); this model is referred to as Model R. This model is not rigid but is practical and simple to calculate; it gives a good approximation of the relation between critical current and damage front at high bending strains, as well as between critical current and bending strain, as shown later in Section 4.3.

3.2.1 Model S

In Model S, the actual shape of the core is used (ABCDEFGHA in Fig. 4(c)), and the y-coordinate of the boundary of the core, y_{core}, is expressed as a function of x with a 9th order polynomial for the present sample.[11,12] The unit of length is millimeters.

$$\left.\begin{aligned}
\text{ABC: } y_{core} &= 0.117324 + 1.13901x + 10.0985x^2 + 38.6006x^3 + 83.9271x^4 \\
&\quad + 113.805x^5 + 97.9306x^6 + 51.8601x^7 + 15.3722x^8 + 1.94706x^9 \\
&\quad \text{for } -1.76 < x < -0.017 \\
\text{CDE: } y_{core} &= 0.0765863 + 0.132501x + 1.36795x^2 - 11.2465x^3 + 36.2954x^4 \\
&\quad - 63.3049x^5 + 64.1326x^6 - 37.7293x^7 + 11.9598x^8 - 1.58008x^9 \\
&\quad \text{for } -0.017 < x < +1.76 \\
\text{EFGHA: } &\text{symmetry of rotation of ABCDE with respect to } x = y = 0
\end{aligned}\right\} \quad (2)$$

Under the applied bending strain, tensile strain is exerted on the filaments in the core along the sample length direction (current transport direction). The exerted tensile strain is dependent on the location; it increases with distance from the neutral axis.[6,11,12] Accordingly, the filaments farthest from the neutral axis, existing at $y_{core} = y_{core,max}$ ($= y_{core,max}$(S) and $y_{core,max}$(R) in Fig. 4(c) for Models S and R, respectively), have the highest tensile strain and are fractured first at

$\varepsilon_B = \varepsilon_{B,irr}$ (the irreversible bending strain at which damage first occurs and critical current reduction starts). When the bending strain is raised from $\varepsilon_{B,irr}$ to $\varepsilon_{B,i}$ and then to $\varepsilon_{B,i+1}$, the damage front y_f extends downward from $y_{core,max}$ to $y_{f,i}$ and then to $y_{f,i+1}$ (Fig. 4(c)). The damage extension leads to reduction in the cross-sectional area of the current transporting Bi2223 filaments and therefore critical current.

Denoting the tensile fracture strain of the filaments under no residual strain as ε_f and the residual strain of the filaments along the sample length direction as ε_r, the damage front y_f is given by[11,12]

$$y_f = \frac{(t/2)(\varepsilon_f - \varepsilon_r)}{\varepsilon_B} \tag{3}$$

The first damage takes place at $y_f = y_{core,max}$ at $\varepsilon_B = \varepsilon_{B,irr}$ as stated above. Substituting $y_f = y_{core,max}$ and $\varepsilon_B = \varepsilon_{B,irr}$ into eq. (3), we obtain the irreversible bending strain $\varepsilon_{B,irr}$ in the following form:

$$\varepsilon_{B,irr} = \left(\frac{t/2}{y_{core,max}}\right)(\varepsilon_f - \varepsilon_r) \tag{4}$$

Because the $\varepsilon_f - \varepsilon_r$ value is different from specimen to specimen and also from position to position within a specimen, the y_f (eq. (3)) and $\varepsilon_{B,irr}$ (eq. (4)) are distributed among the specimens. The normalized critical current I_c/I_{c0} is 1(unity) for $\varepsilon_B \le \varepsilon_{B,irr}$. For $\varepsilon_B \ge \varepsilon_{B,irr}$, the damage front y_f extends downward as stated above, leading to reduction in the cross-sectional area of the current transporting Bi2223 filaments and therefore critical current.

In the Bi2223 composite tape, only the tensile side is damaged up to around 1.0% bending strain, as has been verified by the X-ray diffraction analysis.[18] In the present work, we consider the case where only the core for $y > 0$ (tensile side under the bending strain) is damaged. The experimental results are described for this condition, as shown later in Section 4.2. When all specimens are damaged as in the present case (I_c/I_{c0} values of all specimens are less than unity at $\varepsilon_B = 0.6$, 0.8 and 1.0% (Figs. 1, 2 and 3)), the normalized critical current, I_c/I_{c0}, is expressed by[11,12]

$$\frac{I_c}{I_{c0}} = 1 - \int_{-W_{core}/2}^{W_{core}/2} \left[(t/2)\left\{\frac{y_{core}}{t/2} - \frac{\varepsilon_f - \varepsilon_r}{\varepsilon_B}\right\}\right] dx/A_{core} \tag{5}$$

where A_{core} ($= 0.646\,mm^2$ in the present sample) is the cross-sectional area of the core.

3.2.2 Model R

In Model R, the shape of the core is approximated as a rectangle (abcd in Fig. 4(c)). In this approximation, the width of the core (W_{core} ($= 3.52$ mm) in Fig. 4(c)) and cross-sectional area of the core ($A_{core} = 0.646\,mm^2$) are taken to be same as those of Model S. The x- and y-coordinates of the boundary of the core, x_{core} and y_{core}, respectively, are expressed by eq. (6).[11] The unit of length is millimeters.

$$\left.\begin{aligned} &\text{ab: } y_{core} = 0.0918 \text{ for } -1.76 \le x \le 1.76 \\ &\text{bc: } x_{core} = 1.76 \text{ for } -0.0918 \le y \le 0.0918 \\ &\text{cd: } y_{core} = -0.0918 \text{ for } -1.76 \le x \le 1.76 \\ &\text{da: } x_{core} = -1.76 \text{ for } -0.0918 \le y \le 0.0918 \end{aligned}\right\} \tag{6}$$

The relations among ε_B, $y_f/(t/2)$, $\varepsilon_f - \varepsilon_r$ and $\varepsilon_{B,irr}$ given by eqs. (3) and (4) hold both for Models R and S. Due to the simplification of the shape of the core in Model R, I_c/I_{c0} (<1) expressed by eq. (5) for Model S is reduced to

$$\frac{I_c}{I_{c0}} = \frac{1}{2}\left\{1 + \left(\frac{1}{y_{core,max}/(t/2)}\right)\left(\frac{\varepsilon_f - \varepsilon_r}{\varepsilon_B}\right)\right\} \tag{7}$$

where $y_{core,max} = y_{core,max}(R)$ ($= 0.0918$ mm).

4. Results and Discussion

4.1 Analysis of the distribution of I_c/I_{c0} values by the Weibull approach

When $(I_c/I_{c0})_{min} = 0$ in eq. (1), the parameters to be estimated by the regression analysis are reduced to two ($(I_c/I_{c0})_0$ and m). Such a function has been called a two-parameter Weibull function. In the case of two-parameter Weibull function, the relation of $\ln\ln(1-F)^{-1}$ to $\ln(I_c/I_{c0})$ is linear. If the measured (I_c/I_{c0}) values obey the three-parameter function (eq. (1) with $(I_c/I_{c0})_{min} > 0$), the plot of $\ln\ln(1-F)^{-1}$ against $\ln(I_c/I_{c0})$ is convex.[13] Figure 5(a) shows the plot of $\ln\ln(1-F)^{-1}$ against $\ln(I_c/I_{c0})$, suggesting that the distribution of the I_c/I_{c0} values at $\varepsilon_B = 0.6$, 0.8 and 1.0% are described by the three-parameter Weibull distribution function with $(I_c/I_{c0})_{min} > 0$.

The values of $(I_c/I_{c0})_{min}$, m and $(I_c/I_{c0})_0$ that fit best to the experimental result at each bending strain can be obtained by regression analysis in the following procedure. Taking the data at $\varepsilon_B = 0.6\%$ as an example, the plot of $\ln\ln(1-F)^{-1}$

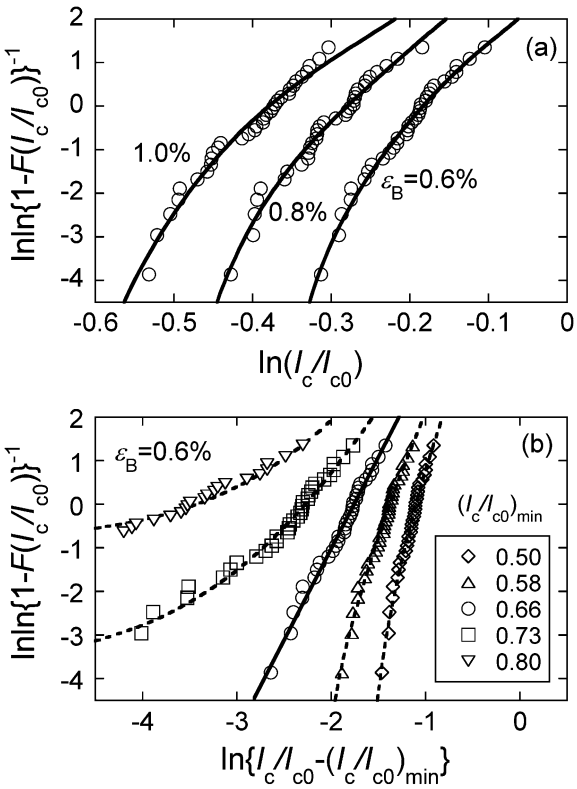

Fig. 5 (a) Plot of $\ln\ln(1-F)^{-1}$ against $\ln(I_c/I_{c0})$ for measured I_c/I_{c0} values at $\varepsilon_B = 0.6$, 0.8 and 1.0%, which are upward convex. (b) Plot of $\ln\ln(1-F)^{-1}$ against $\ln\{I_c/I_{c0} - (I_c/I_{c0})_{min}\}$ for various $(I_c/I_{c0})_{min}$ values for measured I_c/I_{c0} values at $\varepsilon_B = 0.6\%$, as an example. The $\ln\ln(1-F)^{-1} - \ln\{I_c/I_{c0} - (I_c/I_{c0})_{min}\}$ curve is convex when $(I_c/I_{c0})_{min}$ is low ($(I_c/I_{c0})_{min} = 0.50$ and 0.58) but is linear when $(I_c/I_{c0})_{min}$ is 0.66, and is downward concave when $(I_c/I_{c0})_{min}$ is high (0.73 and 0.80).

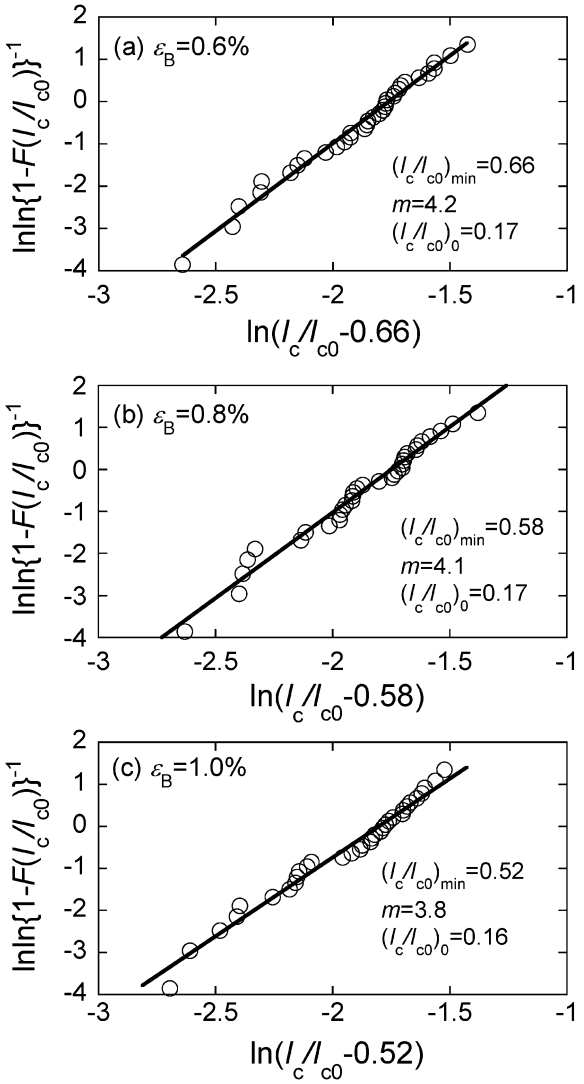

Fig. 6 Plot of $\ln\ln(1-F)^{-1}$ against $\ln\{I_c/I_{c0}-(I_c/I_{c0})_{min}\}$ for $(I_c/I_{c0})_{min}$ values that give the highest linearity between $\ln\ln(1-F)^{-1}$ and $\ln\{I_c/I_{c0}-(I_c/I_{c0})_{min}\}$. ($(I_c/I_{c0})_{min}=0.66$, 0.58 and 0.52 at $\varepsilon_B=0.6$, 0.8 and 1.0%, respectively).

against $\ln\{I_c/I_{c0}-(I_c/I_{c0})_{min}\}$ is convex when the $(I_c/I_{c0})_{min}$ value is low (0.50, 0.58) but is concave when it is high (0.73, 0.80), as shown in Fig. 5(b). Between low and high values of $(I_c/I_{c0})_{min}$, there exists a value of $(I_c/I_{c0})_{min}$ that gives the highest linearity for the relation between $\ln\ln(1-F)^{-1}$ and $\ln\{I_c/I_{c0}-(I_c/I_{c0})_{min}\}$, as shown by the case of $(I_c/I_{c0})_{min}=0.66$ in this example. Once this $(I_c/I_{c0})_{min}$ value is determined, the values of m and $(I_c/I_{c0})_0$ can be obtained from the slope and extrapolation for the plot of $\ln\ln(1-F)^{-1}$ against $\ln\{I_c/I_{c0}-(I_c/I_{c0})_{min}\}$.

Figure 6 shows the plot of $\ln\ln(1-F)^{-1}$ against $\ln\{I_c/I_{c0}-(I_c/I_{c0})_{min}\}$, in which the $(I_c/I_{c0})_{min}$ values that give the highest linearity between the $\ln\ln(1-F)^{-1}$ and $\ln\{I_c/I_{c0}-(I_c/I_{c0})_{min}\}$ were 0.66, 0.58 and 0.52 at $\varepsilon_B=0.6$, 0.8 and 1.0%, respectively. The high linearity between the $\ln\ln(1-F)^{-1}$ and $\ln\{I_c/I_{c0}-(I_c/I_{c0})_{min}\}$ means that the I_c/I_{c0} values are described well by the three-parameter Weibull distribution function. The estimated values of $\{(I_c/I_{c0})_{min}, m, (I_c/I_{c0})_0\}$ were (0.66, 4.2, 0.17), (0.58, 4.1, 0.17) and (0.52, 3.8, 0.16) at $\varepsilon_B=0.6$, 0.8 and 1.0%, respectively.

Substituting the estimated parameter values of $(I_c/I_{c0})_{min}$, m and $(I_c/I_{c0})_0$ into eq. (1), the cumulative probability F–critical current I_c/I_{c0} relations at $\varepsilon_B=0.6$, 0.8 and 1.0% were calculated, as shown by the solid curves in Fig. 2. The measured $F-I_c/I_{c0}$ relations are well described. Moreover, with the estimated parameter values, the cumulative probability given by eq. (1) was converted to the density probability f (frequency). The calculated $f-I_c/I_{c0}$ relations are presented as solid curves in Fig. 3, describing well the experimental results.

As shown above, it was found that the distribution of I_c/I_{c0} values is described well by the three parameter Weibull distribution function. It should be noted that the decrease in $(I_c/I_{c0})_{min}$ with increasing bending strain ε_B, reflecting the extension of the damage front of the most seriously damaged specimen with increasing ε_B, could be estimated by the Weibull approach quantitatively. However, the values of I_c/I_{c0}, m and $(I_c/I_{c0})_0$ were estimated as the fitting parameters at this stage. The physical meaning is discussed in Section 4.3.

4.2 Analysis of the distribution of I_c/I_{c0} values by the damage approach (Model S)

4.2.1 Estimation of distribution of $\varepsilon_f-\varepsilon_r$ values

If the distribution function of the $\varepsilon_f-\varepsilon_r$ values is known in advance, the distribution of I_c/I_{c0} can be calculated by substituting y_{core} (eq. (2)), bending strain ε_B and the known value of A_{core} (0.646 mm^2 in the present sample) into eq. (5). However, the $\varepsilon_f-\varepsilon_r$ value is not known in advance. In the present work, using Model S in which the actual shape of the core was incorporated, the $\varepsilon_f-\varepsilon_r$ values were back-calculated by substituting the following into eq. (5): the measured I_c/I_{c0} values at each bending strain shown in Figs. 2 and 3, the y_{core} expressed by eq. (2), and the measured values of the geometrical parameters ($y_{core,max}=y_{core,max}(S)=0.117$ mm, $W_{core}=3.70$ mm, $t=0.270$ mm and $A_{core}=0.646$ mm^2).

The cumulative probability F of the obtained $\varepsilon_f-\varepsilon_r$ values at $\varepsilon_B=0.6$, 0.8 and 1.0% are presented in Fig. 7(a), (b), (c). The $\varepsilon_f-\varepsilon_r$ value corresponds to the tensile strain at which the Bi2223 filaments in the composite tape fracture. The average of $\varepsilon_f-\varepsilon_r$ value, $(\varepsilon_f-\varepsilon_r)_{ave}$, was 0.25%. The strain at which the filaments in the present composite tape are damaged under applied tensile strain has been estimated to be around 0.25% from the change in the stress carrying capacity upon occurrence of the damage in the stress-strain curve.[6,19] The estimated value $(\varepsilon_f-\varepsilon_r)_{ave}=0.25\%$ in the present work coincides with this value.

The distribution of the obtained $\varepsilon_f-\varepsilon_r$ values was formulated by application of the three-parameter Weibull distribution function, which has widely been used to describe the strength distribution of materials.[15] According to this function, the cumulative probability $F(\varepsilon_f-\varepsilon_r)$ is expressed by

$$F(\varepsilon_f-\varepsilon_r)=1-\exp\left[-\left\{\frac{(\varepsilon_f-\varepsilon_r)-(\varepsilon_f-\varepsilon_r)_{min}}{(\varepsilon_f-\varepsilon_r)_0}\right\}^m\right] \quad (8)$$

where $(\varepsilon_f-\varepsilon_r)_{min}$ is the minimum (lower limit) value of $\varepsilon_f-\varepsilon_r$, and $(\varepsilon_f-\varepsilon_r)_0$ and m are the scale and shape parameters, respectively. From the regression analysis, the values of $(\varepsilon_f-\varepsilon_r)_{min}$, $(\varepsilon_f-\varepsilon_r)_0$ and m were estimated.

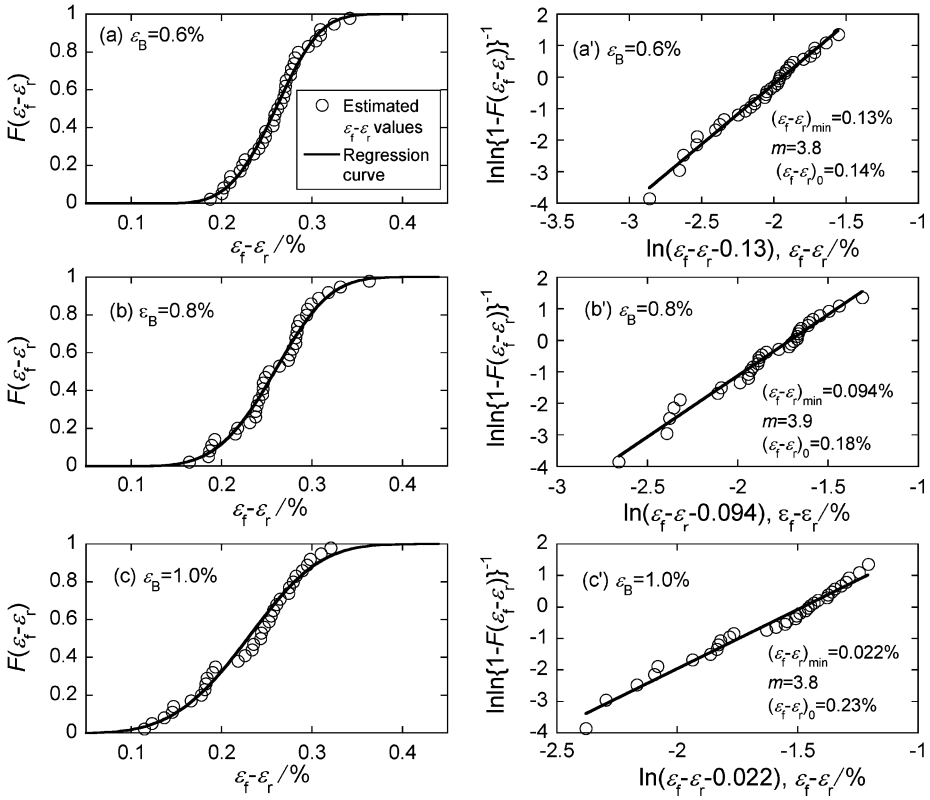

Fig. 7 Cumulative probability F of $\varepsilon_f - \varepsilon_r$ values at ε_B = (a) 0.6, (b) 0.8 and (c) 1.0%, and plot of $\ln\ln(1-F)^{-1}$ against $\ln\{\varepsilon_f - \varepsilon_r - (\varepsilon_f - \varepsilon_r)_{min}\}$ for $(\varepsilon_f - \varepsilon_r)_{min}$ values that give the highest linearity between $\ln\ln(1-F)^{-1}$ and $\ln\{\varepsilon_f - \varepsilon_r - (\varepsilon_f - \varepsilon_r)_{min}\}$ ($(\varepsilon_f - \varepsilon_r)_{min}$ = 0.13, 0.094 and 0.022% at ε_B = (a′) 0.6, (b′) 0.8 and (c′) 1.0%, respectively).

Figure 7(a′), (b′), (c′) shows the plot of $\ln\ln(1-F)^{-1}$ against $\ln\{\varepsilon_f - \varepsilon_r - (\varepsilon_f - \varepsilon_r)_{min}\}$, in which the $(\varepsilon_f - \varepsilon_r)_{min}$ values that gave the highest linearity between $\ln\ln(1-F)^{-1}$ and $\ln\{\varepsilon_f - \varepsilon_r - (\varepsilon_f - \varepsilon_r)_{min}\}$ were input. The high linearity between $\ln\ln(1-F)^{-1}$ and $\ln\{\varepsilon_f - \varepsilon_r - (\varepsilon_f - \varepsilon_r)_{min}\}$ means that the $\varepsilon_f - \varepsilon_r$ values are described well by the three-parameter Weibull distribution function. The estimated values of $\{(\varepsilon_f - \varepsilon_r)_{min}, m, (\varepsilon_f - \varepsilon_r)_0\}$ were (0.13%, 3.8, 0.14%), (0.094%, 3.9, 0.18%) and (0.022%, 3.8, 0.23%) at ε_B = 0.6, 0.8 and 1.0%, respectively. The solid curves in Fig. 7(a), (b), (c) show the results of the regression analysis corresponding to the solid lines in Fig. 7(a′), (b′), (c′), respectively.

4.2.2 Estimation of distribution of I_c/I_{c0} values using the distributed $\varepsilon_f - \varepsilon_r$ values

By combining the distribution function of $\varepsilon_f - \varepsilon_r$ values expressed by eq. (8) with eq. (5), and substituting y_{core} (eq. (2)), the known values of $t/2$, A_{core} and ε_B, and the estimated values of $(\varepsilon_f - \varepsilon_r)_{min}$, m and $(\varepsilon_f - \varepsilon_r)_0$, we numerically calculated the cumulative (F) and density (f) distributions of I_c/I_{c0} at each bending strain. The experimental results are reproduced well. It was confirmed that the present damage approach is a useful tool for reproduction of distribution of I_c/I_{c0} values with high accuracy. Note that the calculation results were very close to the results of the Weibull approach shown with the solid curves in Figs. 2 and 3, and the difference between the damage approach and Weibull approach cannot be distinguished on this scale. This means that (i) the distribution of $\varepsilon_f - \varepsilon_r$ values are estimated accurately in the reverse analysis from distribution of I_c/I_{c0} values to that of $\varepsilon_f - \varepsilon_r$ values through eq. (5) and (ii) the critical current distribution of the I_c/I_{c0} values obtained by using the distributed $\varepsilon_f - \varepsilon_r$ values is expressed by the three-parameter Weibull distribution as well as that obtained by the direct Weibull approach. An example demonstrating (i) and (ii) mentioned above is shown in Fig. 8. For comparison with Fig. 5(b), this figure presents a plot of $\ln\ln(1-F)^{-1}$ versus $\ln\{I_c/I_{c0} - (I_c/I_{c0})_{min}\}$ for various $(I_c/I_{c0})_{min}$ values at ε_B = 0.6%, as calculated with the estimated distribution function of $\varepsilon_f - \varepsilon_r$ values at ε_B = 0.6%. A linear relation

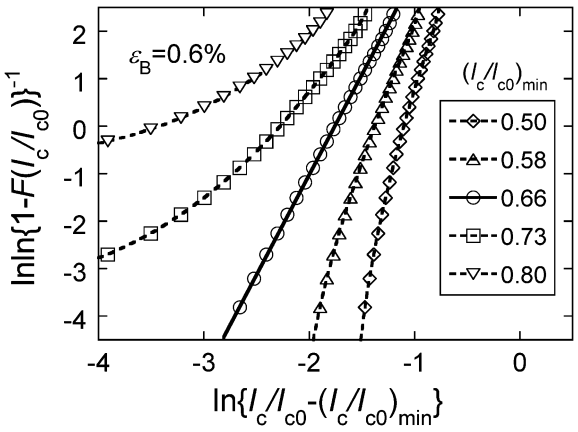

Fig. 8 Plot of $\ln\ln(1-F)^{-1}$ against $\ln\{I_c/I_{c0} - (I_c/I_{c0})_{min}\}$ for different $(I_c/I_{c0})_{min}$-values for distributed I_c/I_{c0} values calculated by substituting the distributed $\varepsilon_f - \varepsilon_r$ values into eq. (5). $(I_c/I_{c0})_{min}$ values used in this figure (0.50, 0.58, 0.66, 0.73 and 0.80) are the same as those used in the plot for measured I_c/I_{c0} values in Fig. 5(b).

the same as that in Fig. 5(b) is actually obtained for $(I_c/I_{c0})_{min} = 0.66$. The m and $(I_c/I_{c0})_0$ values are found to be 4.2 and 0.17, respectively, for $(I_c/I_{c0})_{min} = 0.66$, which are the same as those obtained by the direct Weibull approach shown in Fig. 6(a).

Here, the important finding is that the distribution function of the measured damage-controlled I_c/I_{c0} values, as expressed by the three-parameter Weibull distribution, can be reproduced accurately by the distribution of the damage-controlling $\varepsilon_f - \varepsilon_r$ values, as expressed by the three-parameter Weibull distribution. This result suggests the followings. (a) The distribution of the critical current of bent-damaged specimens is accounted for from the viewpoint of the difference in damage evolution among the specimens. (b) In the Weibull approach, the parameters of $(I_c/I_{c0})_{min}$, m and $(I_c/I_{c0})_0$ were obtained as the fitting parameters, but the physical significance was unknown. The correlation of the distribution of I_c/I_{c0} values to the distribution of $\varepsilon_f - \varepsilon_r$ values obtained in the present work demonstrates that the parameters obtained by the Weibull approach surely reflect the difference in the damage extent among the specimens.

As shown above, using Model S for the damage approach, we observed the correlation of distribution of $\varepsilon_f - \varepsilon_r$ values, which are related to the distribution of the damage front as indicated by eq. (3), to the distribution of I_c/I_{c0} values. However, if only the Model S is used, only numerical calculation can be conducted. Accordingly, it is difficult to formulate a direct correlation of the distribution of $\varepsilon_f - \varepsilon_r$ values to the distribution of I_c/I_{c0} values.

In the next sub-section, Model R is used for the damage approach to find the correspondence of the $(\varepsilon_f - \varepsilon_r)_{min}$, m and $(\varepsilon_f - \varepsilon_r)_0$ values (which characterize the distribution of damage evolution), to the $(I_c/I_{c0})_{min}$, m and $(I_c/I_{c0})_0$ values (which characterize the distribution of critical current).

4.3 Derivation of three parameter Weibull distribution function for I_c/I_{c0} values from the damage approach using Model R

4.3.1 Difference and similarity in I_c/I_{c0} values between Models S and R

In Model R, the shape of the core is approximated as a rectangle (Fig. 4(c)). The accuracy in calculation with this model is lower than that with Model S, in which the actual shape of the core is incorporated. In this subsection, the difference and similarity in I_c/I_{c0} values between Models S and R are examined in advance of application of Model R.

When the $\varepsilon_f - \varepsilon_r$ value is known, the I_c/I_{c0} at $\varepsilon_B \geq \varepsilon_{B,irr}$ can be calculated by eqs. (5) and (7) for Models S and R, respectively. $\varepsilon_{B,irr}$ can be calculated using eq. (4) with $y_{core,max}/(t/2) = 0.87$ and 0.68 for Models S and R, respectively. As the average of $\varepsilon_f - \varepsilon_r$ values, $(\varepsilon_f - \varepsilon_r)_{ave}$, was 0.25%, the average irreversible bending strain $\varepsilon_{B,irr,ave}$ is calculated to be 0.29 and 0.37% for Models S and R, respectively. Figure 9 shows the calculated variation of average of I_c/I_{c0} values, $(I_c/I_{c0})_{ave}$, for bending strain ε_B. The calculated values of $(I_c/I_{c0})_{ave}$ at $\varepsilon_B = 0.6$, 0.8 and 1.0% calculated using Models S and R are almost the same, while the values of $(I_c/I_{c0})_{ave}$ at lower bending strain differ between the models (values of $\varepsilon_{B,irr,ave}$ and $(I_c/I_{c0})_{ave}$ at $\varepsilon_B = 0.4\%$ are overestimated by Model R) due to the simplification of the shape of the core in Model R. Because the critical current I_c/I_{c0} at $\varepsilon_B = 0.6$, 0.8 and 1.0% is well expressed in a simple form by eq. (7) in Model R, eq. (7) is used for formulation of distribution of I_c/I_{c0} values at these high bending strains.

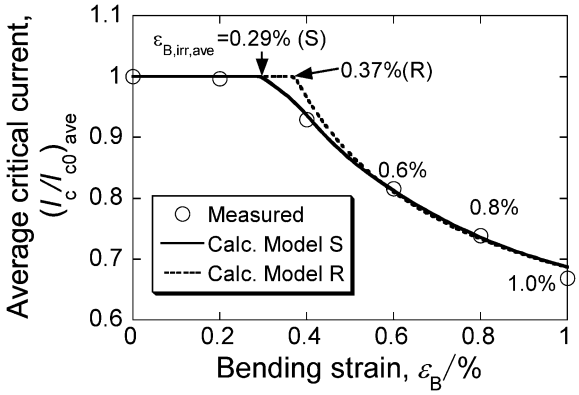

Fig. 9 Measured and analyzed change in average critical current $(I_c/I_{c0})_{ave}$ with bending strain ε_B. Results analyzed using Models S and R for $(\varepsilon_f - \varepsilon_r)_{ave} = 0.25\%$ are shown as solid and broken curves, respectively. Average irreversible bending strains ($\varepsilon_{B,irr,ave}$) analyzed using Models S (0.29%) and R (0.37%) are indicated with arrows.

4.3.2 Derivation of distribution function of I_c/I_{c0} values using Model R

The I_c/I_{c0} for $\varepsilon_B \geq \varepsilon_{B,irr}$ expressed by eq. (7) in Model R is dependent on the $\varepsilon_f - \varepsilon_r$ value, which is distributed according to eq. (8). Substituting $\varepsilon_f - \varepsilon_r = \{2(I_c/I_{c0}) - 1\}\varepsilon_B\{y_{core,max}(R)/(t/2)\}$ derived from eq. (7) into eq. (8), we have

$$F(I_c/I_{c0} \text{ at } \varepsilon_B) = 1 - \exp\left[-\left\{ \frac{I_c/I_{c0} - \left(\frac{1}{2} + \frac{(\varepsilon_f - \varepsilon_r)_{min}/(2\varepsilon_B)}{y_{core,max}(R)/(t/2)} \right)}{\frac{(\varepsilon_f - \varepsilon_r)_0/(2\varepsilon_B)}{y_{core,max}(R)/(t/2)}} \right\}^m \right]. \quad (9)$$

In a comparison of eq. (9) with eq. (1), eq. (9) is simply a form of the three parameter Weibull distribution for I_c/I_{c0} values with the correspondence of

$$(I_c/I_{c0})_{min} = \frac{1}{2} + \frac{(\varepsilon_f - \varepsilon_r)_{min}/(2\varepsilon_B)}{y_{core,max}(R)/(t/2)} \quad (10)$$

$$(I_c/I_{c0})_0 = \frac{(\varepsilon_f - \varepsilon_r)_0/(2\varepsilon_B)}{y_{core,max}(R)/(t/2)} \quad (11)$$

$$m\ (I_c/I_{c0} \text{ distribution}) = m\ (\varepsilon_f - \varepsilon_r \text{ distribution}). \quad (12)$$

Substituting the parameter values of $(\varepsilon_f - \varepsilon_r)_{min}$, $(\varepsilon_f - \varepsilon_r)_0$ and m for the $\varepsilon_f - \varepsilon_r$ distribution estimated by the statistical analysis of $\varepsilon_f - \varepsilon_r$ values in the damage approach [$\{(\varepsilon_f - \varepsilon_r)_{min}, m, (\varepsilon_f - \varepsilon_r)_0\}$ = (0.13%, 3.8, 0.14%), (0.094%, 3.9, 0.18%) and (0.022%, 3.8, 0.23%) at $\varepsilon_B = 0.6$, 0.8 and 1.0%, respectively], and $y_{core,max}(R)/(t/2) = 0.68$ into eqs. (10), (11) and (12), we obtained the $(I_c/I_{c0})_{min}$, m and $(I_c/I_{c0})_0$ values for the distribution of I_c/I_{c0} values, as shown in Table 1. The parameter values calculated by the damage approach with Model R are almost the same as those estimated by the Weibull approach. A direct comparison of the calculated cumulative probability F and probability

Table 1 Estimated values of $(I_c/I_{c0})_{min}$, I_0 and m from the direct Weibull approach and damage approach with Model R (eq. (9)) at $\varepsilon_B = 0.6$, 0.8 and 1.0%.

Parameter		$(I_c/I_{c0})_{min}$		$(I_{0c}/I_{c0})_0$		m	
Approach		Weibull	Damage	Weibull	Damage	Weibull	Damage
ε_B (%)	0.6	0.66	0.66	0.17	0.18	4.2	3.8
	0.8	0.58	0.59	0.17	0.17	4.1	3.9
	1.0	0.52	0.52	0.16	0.17	3.8	3.8

density f of I_c/I_{c0} values using eq. (9) based on the damage approach using Model R with the measured ones is shown in Figs. 2 and 3, where the calculation results are presented as broken curves. As shown above, the calculated $F(I_c/I_{c0})$ (and $f(I_c/I_{c0})$) curves based on the damage approach with Model S and direct Weibull approach are similar and the difference between them cannot be distinguished. The experimental results are described well also by the damage approach with Model R. The slight difference at lower ε_B (0.6 and 0.8%) between the damage approach with Model S (and the Weibull approach) and the damage approach with Model R stems from the simplification of the shape of the core in Model R.

It is important to note that the value of m for distribution of I_c/I_{c0} is the same as that for the distribution of $\varepsilon_f - \varepsilon_r$ values (eq. (12)) in Model R. $\varepsilon_f - \varepsilon_r$ refers to the tensile fracture strain in the core of the Bi2223 filaments. The value of m is a measure of the coefficient of variation of the $I_c/I_{c0} - (I_c/I_{c0})_{min}$ as well as that of $\varepsilon_f - \varepsilon_r - (\varepsilon_f - \varepsilon_r)_{min}$; for smaller m, the distribution of the values of $I_c/I_{c0} - (I_c/I_{c0})_{min}$ and $\varepsilon_f - \varepsilon_r - (\varepsilon_f - \varepsilon_r)_{min}$ is smaller. Equation (12) indicates that the coefficient of variation of the normalized critical current distribution is governed by the difference in damage evolution among the specimens stemming from the distributed $\varepsilon_f - \varepsilon_r$ values. As the distribution of $\varepsilon_f - \varepsilon_r$ values follows the three-parameter Weibull distribution, the I_c/I_{c0} values also follows the same type distribution function. In this way, the reason why the distribution of I_c/I_{c0} values of bent-damaged specimens is described by the three-parameter Weibull distribution function is accounted for by the difference in damage evolution among the specimens.

5. Conclusions

(1) The distribution of the measured normalized critical current values of the Bi2223 composite tape (VAM1 sample) bent by 0.6, 0.8 and 1.0% in a round robin test of VAMAS/TWA16 were described by the three-parameter Weibull distribution function.

(2) The distribution of the measured normalized critical current values was also described well by the damage evolution approach, in which the difference in damage evolution among the specimens was correlated to the distribution critical current values. From this approach, the Weibull distribution function for critical current values was derived, which gave almost the same parameter values of minimum critical current, scale parameter and shape parameter as those obtained by the direct application of the Weibull distribution function to the experimental results.

(3) Based on the results (1) and (2) above, the reason why the normalized critical current values of bent-damaged composite tape is described by the three-parameter Weibull distribution function was accounted for in a quantitative manner by the difference in damage evolution among the specimens.

Acknowledgement

The authors wish to express their gratitude to The Ministry of Education, Culture, Sports, Science and Technology, Japan, for a grant-in-aid for scientific research.

REFERENCES

1) H. Kitaguchi, K. Itoh, H. Kumakura, T. Takeuchi, K. Togano and H. Wada: IEEE Trans. Appl. Supercond. **11** (2001) 3058–3061.
2) R. Passerini, M. Dhalle', E. Giannini, G. Witz, B. Seeber and R. Flükiger: Physica C **371** (2002) 173–184.
3) H. W. Weijers, J. Schwartz and B. ten Haken: Physica C **372–376** (2002) 1364–1367.
4) K. Osamura, M. Sugano and K. Matsumoto: Supercond. Sci. Technol. **16** (2003) 971–975.
5) H. S. Shin and K. Katagiri: Supercond. Sci. Technol. **16** (2003) 1012–1018.
6) S. Ochiai, T. Matsuoka, J. K. Shin, H. Okuda, M. Sugano, M. Hojo and K. Osamura: Supercond. Sci. Technol. **20** (2007) 1076–1083.
7) S. Ochiai, J. K. Shin, S. Iwamoto, H. Okuda, S. S. Oh, D. W. Ha and M. Sato: J. Appl. Phys. **103** (2008) 123911 (8 pp).
8) S. Ochiai, H. Rokkaku, J. K. Shin, S. Iwamoto, H. Okuda, K. Osamura, M. Sato, A. Otto and A. Malozemoff: Supercond. Sci. Technol. **21** (2008) 075009 (13pp).
9) K. Katagiri, H. S. Shin, K. Kasaba, T. Tsukinokizawa, K. Hiroi, T. Kuroda, K. Itoh and H. Wada: Supercond. Sci. Technol. **16** (2003) 995–999.
10) T. Kuroda, *et al.*: Physica C **425** (2005) 111–120.
11) S. Ochiai, J. K. Shin, H. Okuda, M. Sugano, M. Hojo, K. Osamura, T. Kuroda, K. Itoh and H. Wada: Supercond. Sci. Tecnol. **21** (2008) 054002 (14pp).
12) S. Ochiai, H. Okuda, M. Sugano, M. Hojo, K. Osamura, T. Kuroda, K. Itoh, H. Kitaguchi, H. Kumakura and H. Wada: Supercond. Sci. Technol. **23** (2010) 025006 (12 pp).
13) S. Ochiai, M. Fujimoto, H. Okuda, S. S. Oh and D. W. Ha: J. Appl. Phys. **105** (2009) 06912 (8pp).
14) S. Ochiai, M. Fujimoto, J. K. Shin, H. Okuda, S. S. Oh and D. W. Ha: J. Appl. Phys. **106** (2009) 103916 (11 pp).
15) W. Weibull: J. Appl. Mech. **28** (1951) 293–297.
16) T. Kiss, T. Matsushita and F. Irie: Supercond. Sci. Technol. **12** (1999) 1079–1082.
17) M. Ahoranta, J. Lehtonen, P. Kováč, I. Hušek and T. Melišek: Physica C **401** (2004) 241–245.
18) H. Okuda, J. K. Shin, S. Iwamoto, K. Morishita, Y. Mukai, H. Matsubayashi, S. Ochiai, A. Otto, E. J. Harley, A. Malozemoff and M. Sato: Scr. Mater. **58** (2008) 687–690.
19) S. Ochiai, H. Okuda, M. Sugano, M. Hojo and K. Osamura: J. Appl. Phys. **107** (2010) 083904 (9pp).